JOURNAL OF GEOPHYSICAL RESEARCH, VOL. 106, NO. A3, PAGES 3859-3871, MARCH 1, 2001

Wideband bursts of auroral kilometric radiation and their association with UV auroral bulges

J. Hanasz,[1] H. de Feraudy,[2] R. Schreiber,[3] G. Parks,[4] M. Brittnacher,[4] M. M. Mogilevsky,[5] and T. V. Romantsova[5]

Abstract. Impulsive wideband bursts of auroral kilometric radiation (AKR) observed from the Interball 2 spacecraft are characterized by a rapid rise of intensity (< 1 min) over a wide frequency range from 30 to 900 kHz, followed by a decay over a few minutes. Their source regions expand rapidly both upward and downward along the auroral field lines. The expansion velocity is determined from the rapid broadening of the frequency range of their leading edge (sometimes more than 100 kHz s^{-1}). The drifts can be negative or positive. Above 500 kHz the inferred downward source expansion is sometimes as small as 2 km s^{-1} (at altitudes below 3000 km), much smaller than the velocity of the ion sound waves. In the medium frequency range 200 - 500 kHz (3000 - 6000 km) the expansion velocities are usually large, sometimes more than 3000 km s^{-1}, comparable to the velocity of the Alfvén waves. In the lower frequency range, below 200 kHz (> 6000 km), the bursts show an upward source expansion, often simultaneous with the downward expansion of the same source below 3000 km. We observe a close association of the AKR bursts with the fast expansion of the auroral bulges recorded with the UV imager on Polar. It is concluded that the bursts are triggered during the rapid development of auroral substorms. The bursts show a microstructure, which consists of multiple microbursts lasting sometimes less than 6 s. They indicate that the source regions are filamented. This filamentation may be the counterpart of a filamentary nature of the currents closing the current wedge, flowing parallel to the geomagnetic field.

1. Introduction

The auroral kilometric radiation (AKR) discovered by *Benediktov et al.* [1965] is observed most often at frequencies from 30 kHz to ~ 1 MHz. It originates from the nightside auroral magnetosphere [*Gurnett*, 1974; *Kurth et al.*, 1975]. It is now well established that this radiation is emitted at the electron gyrofrequency [*e.g. Benson and Calvert*, 1979; *Bahnsen et al.*, 1989]; thus its sources must extend from ~ 2000 km to 20000 km above the Earth's surface. Among a number of mechanisms invoked for the AKR generation, the most widely accepted one relies on the electron cyclotron maser instability (CMI), proposed by *Wu and Lee* [1979]. In this mechanism the kinetic energy of the electrons accelerated transversally to the geomagnetic field, to energies ranging from 1 to 10 keV, is converted to electromagnetic extraordinary or ordinary waves at a frequency extremely close to the electron gyrofrequency. This conversion takes place during processes associated with the geomagnetic substorms. The AKR relationship with discrete auroral structures was discovered by *Gurnett* [1974], and its correlation with auroral magnetic activity was statistically proven by *Voots et al.* [1977], *Kaiser and Alexander* [1977], *Green et al.* [1982], and *Benson and Akasofu* [1984]. Excellent examples of AKR sources traced along their field lines to the bright auroral arcs were shown by *Huff et al.* [1988]. A correlation of AKR with the 2 - 12 keV x-ray flux of aurora, based on Polar observations, is reported by *Imhof et al.* [1998]. The first crossing of an AKR source by a spacecraft was shown by *Benson and Calvert* [1979]. Until now the association of the AKR with auroral structures has been best illustrated with the observations of the Viking spacecraft, where UV images of the aurora were available. On several occasions, source crossings were observed precisely at times when the footprint of the spacecraft field line crossed the auroral arcs [*de Fer-*

[1]Space Research Center, Polish Academy of Sciences, Torun.

[2]Centre d'Etude des Environnements Terrestre et Planetaires, CNRS, Velizy, France.

[3]Copernicus Astronomical Center, Polish Academy of Sciences, Torun.

[4]University of Washington, Geophysics Program, Seattle.

[5]Space Research Institute, Russian Academy of Science, Moscow.

Paper number 2000JA900098.
0148-0227/01/2000JA900098$09.00

audy et al., 1987a]. The source crossings by FAST (Fast Auroral Snap shoT) spacecraft [*Ergun et al.*, 1998] confirmed the earlier observations [*de Feraudy et al.*, 1987a] that the AKR sources are density-depleted cavities extending 30 to 300 km in latitude, in which cold electrons are nearly expelled, and that the AKR wave field has electromagnetic character. Waves observed by *Ergun et al.*, [1998] have much higher amplitudes than those observed by Viking.

Most often, the AKR events were reported as being long-duration activity, lasting sometimes for hours, in rather slowly varying frequency ranges. What we present in this paper is quite a different pattern. We show impulsive emissions of AKR, very rapidly reaching broad frequency ranges, growing and decaying in tens of minutes. We also show that they are closely associated with the expansion phase of magnetospheric substorms, manifested by the rapid development of an auroral bulge. This is clearly demonstrated by sequences of images taken by the UV imager aboard Polar.

These impulsive emissions, called wide band bursts of AKR (WBB-AKR), are occasionally distinguished among other radio emissions showing a variety of spectral structures, including the long lasting AKR, which are commonly observed in the range from 30 to 900 kHz with the POLRAD (POLarization of RADioemission) radio spectrograph aboard Interball 2. The WBB-AKR are manifested by a sudden commencement (< 1 min) of the emission over a wide frequency range, followed by a decay lasting for $\sim$ 10 min or more. Although they must have been observed in dynamic spectra obtained from other spacecraft, apparently not much attention has been paid to them. *Morioka et al.* [1981] showed one in the Jikkiken (Exos B) spectra and described it as a sudden expansion of observed emission bandwidth (see their Figure 5). Also, behavior of some AKR events described by *Kaiser and Alexander* [1977], namely, their rapid intensification and bandwidth broadening as functions of substorm phase, resembles spectral and temporal features of WBB-AKR shown in this paper. We must mention the low frequency bursts, sometimes called the terrestrial type III bursts (because of their similarity to the solar type III bursts), which are observed between 30 and 100 kHz [*Anderson et al.*, 1996; *Desch*, 1996; *Steinberg et al.*, 1988]. They have different spectral characteristics, but our observations suggest their association with the WBB-AKR, which needs to be studied. Some of them extend in frequency up to 500 kHz, with unmeasurable frequency drift at higher frequencies [*Kaiser et al.*, 1996]. We note their similarity to WBB-AKR.

In this paper we concentrate on observational features of the WBB-AKR and their association with UV auroral events. The paper is organized as follows. In section 2 we present observations of the AKR bursts and their features. In section 3 we show the association of the WBB-AKR with the rapid expansion of UV auroral bulges observed with the ultraviolet camera [*Torr et al.*, 1995] aboard the Polar spacecraft [*Acuña et al.*, 1995]. In section 4 we discuss the observed features of the AKR bursts in terms of the general knowledge of AKR and substorms. In section 5 we present our conclusions.

2. Observations of AKR Bursts

Interball 2 was launched on August 29, 1996, to an orbit with apogee 19140 km, perigee 780 km, inclination to the equator 62.8°, and nodical period 5.9 hours [*Galeev et al.*, 1995; *Zelenyi and Sauvaud*, 1998]. It is spinning with a period of 120 s, around an axis directed to the Sun. POLRAD is a step frequency analyzer, swept over one of two frequency ranges: 4 kHz to 1 MHz, or 4 kHz to 0.5 MHz, with repetition periods of 6 or 12 s and a frequency resolution of 4.096 kHz [*Hanasz et al.*, 1998a]. The receiver stays at each frequency step for 25 ms or 50 ms, depending on the operation mode; the time constant of the output filter is 6 ms. Three independent channels allow reception of signals from three perpendicular antennas: one located along the spin axis (11 m long) and two others (22 m) located in the plane perpendicular to it. One mode of POLRAD operation is devoted to measurements of the wave polarization.

In preflight calibrations a special care was put on the nonlinear effects produced in the receiver at sum and difference frequencies of an input signal, when its amplitude exceeded some instrumental level. The threshold of this nonlinearity was determined on a level of 63 dB of the total integrated input signal over the receiver level. In the most sensitive mode of POLRAD operation (input attenuation 0 dB) the effect was easily recognized as a frequency broadening of a signal whenever a sufficiently strong AKR emission was met. This broadening was fully reduced by introducing the attenuation of 20 dB between the antennas and the receiver in the operational mode, which covered most of the observational time. To avoid damage from the radiation belts most of POLRAD observations are carried out generally at L shells > 4.5, that is, within the auroral zone and above the polar cap.

From the start of Interball 2 operation through December 31, 1997, we have identified 123 intense and relatively separable bursts of AKR. Their intensity, sometimes exceeding 10^{-14} W m^{-2} Hz^{-1}, is well above the AKR background, usually by more than an order of magnitude. Sometimes they are observed as isolated spectral structures, without any detectable background AKR emission. Their polarization, as measured by POLRAD, is in the righthand extraordinary mode, the same as that for the background AKR.

Spectral features of WBB-AKR are shown in Plate 1. They are characteristic for a sudden increase of their intensity over a wide frequency range, so that the maximum is usually reached in less than 1 min. It is followed by the intensity decrease observed for the order of 10 min in the main part of the bursts. These features are

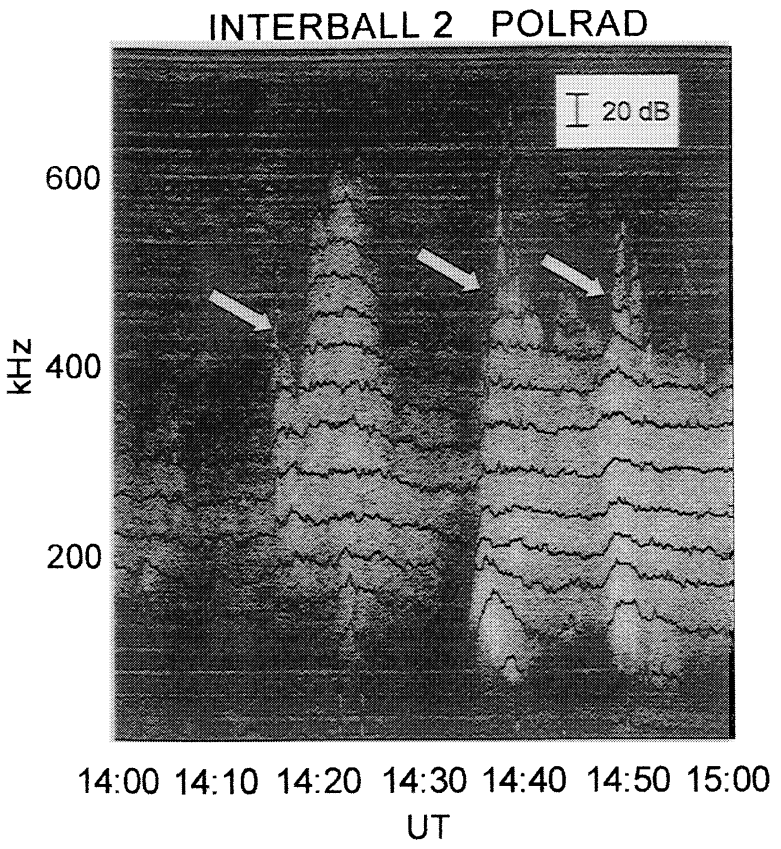

Figure 1. Intensity profiles for a series of auroral kilometric radiation (AKR) bursts on November 18, 1997, superimposed on the AKR dynamic spectrum. The intensities are integrated over a bandwidth of 41 kHz. The lowest profile shows intensity variations for the lowest bandwidth 4 - 45 kHz.

illustrated in Figure 1, which shows the dynamic spectrum of the three AKR bursts with stacked intensity profiles superimposed on it. The profiles are integrated over subsequent 41 kHz frequency bands.

Some well defined events clearly show rise times as short as 6 s, the repetition period of the step frequency analyser (SFA) (Plate 1a). Sometimes they initiate AKR activity lasting for several hours. They appear in the frequency range between 30 and 900 kHz and are characterized by fast frequency drifts of their leading edges, often exceeding 100 kHz s^{-1} and sometimes having unmeasurably high values. The WBB-AKR can be grouped into four classes according to the drift rates of their front edge: (1) unmeasurably high (Plate 1a), (2) negative (Plate 1b), (3) positive (Plate 1c), and (4) bow (with positive and negative drift) (Plate 1d). An additional, fifth class must be introduced, but it will not be discussed here. It consists of bursts accompanied by a simultaneous detached bright dots at the lowest frequencies (Plate 1e). They are shaped like an exclamation sign. These bursts, like the ordinary bursts, can also have different drifts of their main body. The dots are narrow frequency bands 10 to 30 kHz wide, centered usually at frequencies between 30 and 100 kHz and lasting for the order of a minute. Sometimes they are connected with the main burst bodies by bridges of weaker emission.

Plate 1a shows a sudden increase of emission over a frequency range from 150 to 700 kHz, within 6 s, one period of the frequency sweep of the instrument. The estimated drift rate was then > 100 kHz s^{-1}, which corresponds to the expansion velocity of the AKR source exceeding 1700 km s^{-1} along the field line, assuming generation at the gyrofrequency of electrons. The direction of the expansion cannot be determined for this case. Plate 1b shows a burst with a negative frequency drift of ~ 8 kHz s^{-1}, corresponding to the velocity of an upward source expansion of 200 km s^{-1}. Plate 1c presents a burst with a positive frequency drift of 3 kHz s^{-1}. The time difference between the upper and lower parts of the burst determines the drift timescale. For this burst it was 2.5 min. The estimated source expansion was 30 km s^{-1} downward. Plate 1d is an example of a burst with the front edge shaped as a bow. The corresponding source expansion begins at a frequency of ~ 400 kHz (the source is located ~ 4700 km above the Earth's surface) and develops upward and downward with velocities of 50 and 20 km s^{-1}, respectively. The distribution of the source expansion velocities derived from average burst drift rates is shown in Table

Table 1. Source Expansion Velocities Derived From Burst Drift Rates

Drift Type	Drift km s^{-1}	Cases (All)	Exclamation
Non-measurable	> 3000	46	19
Negative	2-1000	23	6
Positive	5-1000	23	9
Bow	10 to > 3000	25	1
Irregular	-	1	0
Undetermined	?	5	4
All together		123	39

1. Generally, the drift rates of the leading edge of the bursts vary with frequency. Most often the edge structure can be divided into three parts according to the drift rates: the center frequency range (approximately from 200 to 500 kHz) with the highest drift, the upper frequency range (above ~ 500 kHz) with positive drift, and the lower range (below ~ 200 kHz) with negative drift. The leading edge usually appears first in the center frequency range (200 to 500 kHz). For the corresponding range of source altitudes, 3000 - 6000 km, the expansion velocities were often large and sometimes nonmeasurable, above 3000 km s^{-1} (see Table 1), comparable to the Alfvén velocity (the order of 10,000 km s^{-1}). In this case the timescale of the frequency drift, defined as a time difference between the earliest and latest time of the drifting edge, was as short as 6 s (a period of sweep repetition). The longest observed drift timescale was 3 min. The drift timescale of the WBB-AKR can range therefore from 6 s to 3 min.

The upper parts of the bursts extend from ~ 500 to 800 kHz. One striking feature is that WBB-AKR are generally standing out from the background AKR emission, not only in intensity but also in a frequency range (see Plate 1c, Figure 1 and Figure 2, Plate 2 b (1510 and 1554 UT)). Their peak frequencies, 700 - 800 kHz, are above the upper cutoffs of the background AKR, while the lowest ones are often below its lower cutoffs. The altitudes of the source bottoms corresponding to the upper cutoffs are between 1200 and 2600 km, lower than the source altitude for the background AKR.

Plates 1 and 2 and Figures 1 and 2 show that the upper parts are much shorter in time and sharper than the medium and lower parts. Here the intensity of the AKR bursts can abruptly increase and further abruptly decrease by 1 - 3 orders of magnitude in time of 1 to several frequency sweeps of the SFA (timescale of 10 s) (see, for example, Plate 1a and Figure 1). In the frequency domain the emission cuts off in one to several frequency steps of 4.096 kHz. Similar upper frequency

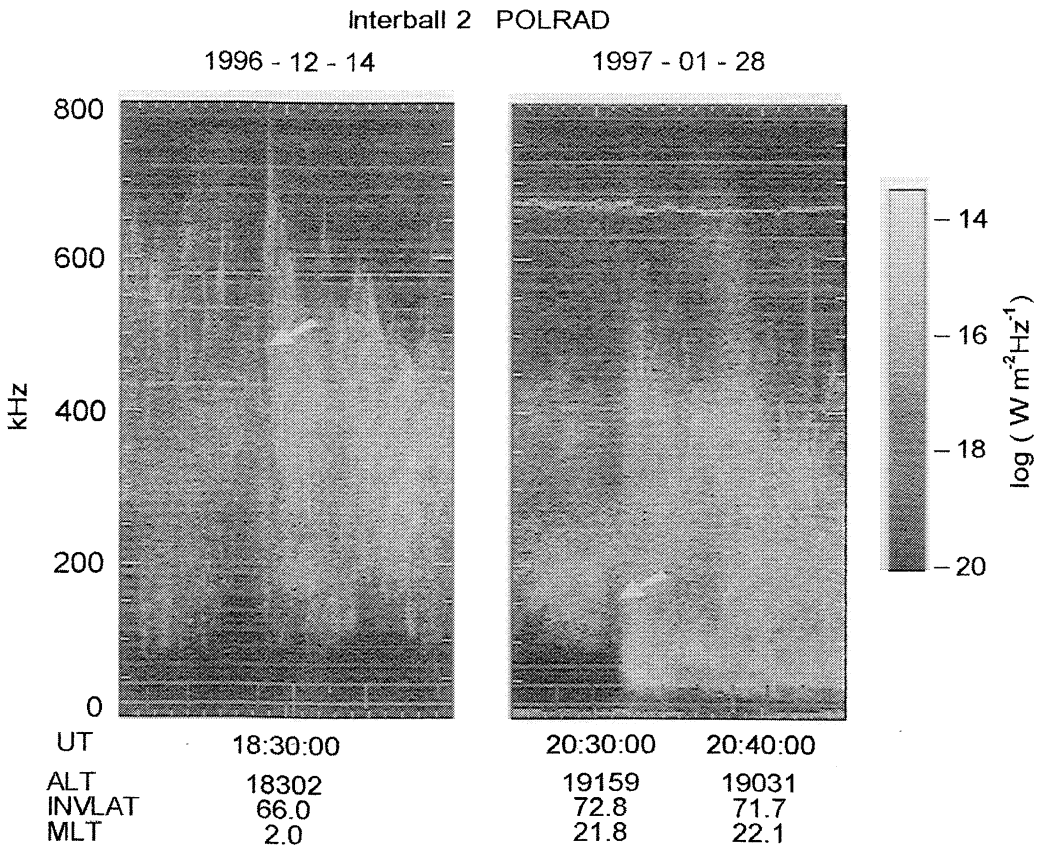

Figure 2. Examples of high-frequency drift rates, at (left) a high frequency part of the burst, and (right) a low frequency part of the burst.

cutoffs have already been found for the AKR emission by *Hanasz et al.* [1998b]. The burst peaks are sharp, often lasting no longer than one frequency sweep. The timescale of intensity variations at upper frequencies is estimated to be of the order of 10 s.

The summary of temporal characteristics of WBB-AKR is as follows: The rise time is < 1 min for the main part of the bursts, except for the upper frequency part where it is ~ 10 s; the decay time is of the order of 10 min for the main part, except for the upper frequency part where it becomes ~ 10 s; and the drift timescale is 6 - 180 s, of the order of 1 min.

The upper frequency parts of the bursts, from 500 to 800 kHz, have been analyzed in detail for 13 cases. Over this small sample, it appears that the leading and trailing edges of the source region move much slower than those of the medium-frequency range, with velocities of the order of 3 - 30 km s^{-1}. Their downward velocities, corresponding to increasing frequencies, are generally higher than the upward ones of the trailing edges: on the average, 14.3 against 10 km s^{-1}. However, on some occasions the reverse is observed. The edges are sharp and well defined, and the expansion velocities can be measured with a relative accuracy of 17%, much better than the dispersion of the values, which is 7.5 km s^{-1} over 28 samples. For example, in one case the velocity was as low as 2.3 km s^{-1}. One striking feature is that on many occasions the velocity stays fairly constant over an altitude range spanning over 500 km and sometimes up to 1000 km.

In the lower frequency range, below 200 kHz, the leading edges usually present a negative frequency drift, which may correspond to an upward expansion of the source region, simultaneous to the downward expansion of its lower edge. However, care must be taken when the altitude of the source region is comparable to that of the spacecraft. Then, since the AKR rays are emitted inside a cone with an axis along the magnetic field and with an opening angle less than 90°, the access of the AKR to the spacecraft can be subjected to geometrical constraints, which give rise to dispersion features on the spectrograms. At the lowest frequencies the decay time is often shorter than that at medium frequencies; however, this may be the effect of a limited propagation cone.

The border frequencies between the three ranges described above are highly variable. In some events (see Figure 2, left) this upper frequency part is absent, and the upper frequency of the medium range becomes the highest frequency of the burst (800 kHz). The corresponding expansion velocity is high (above 3000 km s^{-1}). Sometimes the medium part can broaden downward, below 100 kHz, equivalent to a source altitude above $\sim$ 10,000 km (see Figure 2, right).

The bow-shaped bursts in Plate 1d, is characteristic for double-sided expansion of the AKR source region. They show that the first excitation of the source region takes place in the medium altitude range of $\sim$ 4000 km (corresponding to 400 kHz), and the excitation further proceeds simultaneously upward and downward. For the case of the bow shown in Plate 1d the expansion velocities are 24 and 35 km s^{-1}, respectively.

The Plasma Wave Instrument step frequency receiver (SFR-A) [*Gurnett et al.*, 1995] aboard the Polar spacecraft [*Acuña et al.*, 1995] has recorded a number of WBB-AKR simultaneously with POLRAD. An example in Plate 2 shows a detailed similarity in the spectra of the same bursts recorded by both spacecraft, separated by an angular distance of 18° and by a spacing of 36,000 km. Such similarity can be governed only by the time-varying source structure and not by the AKR propagation particularities. The first strongest burst of Plate 2 beginning at 1511 UT is identified as "an exclamation sign burst". Its detached dot was not generated locally around the spacecraft since it was simultaneously observed from Polar and Interball 2. Moreover, its lower frequency was higher than the electron gyrofrequency at the Interball 2 altitude. However, detailed comparison of the bursts recorded on both spacecraft shows that the frequency extent of the AKR bursts observed from the Interball 2 orbit is generally different from that observed from Polar. This indicates that the wave propagation may play a role in limiting the upper and lower frequencies of the bursts.

Though the burst spectra are strongly variable in time, they are weakly structured in frequency, since they do not show any narrowband emissions. Some of their dynamic spectra show that they are the superposition of a number of thin individual microbursts, with a duration (at upper frequencies) comparable to or shorter than a single-frequency sweep time (6 s). This gives the dynamic spectra the appearance of vertical striation (Figure 3). This spiky structure is clear at the highest frequencies (above 550 kHz), where the microbursts stand out from the background. Below this frequency the microbursts seem to merge. However, their traces are sometimes still visible in the lower frequency part. The implications of this fine structure are discussed in section 4.3.

Magnetic local time (MLT) positions of Interball 2 at times of WBB-AKR are shown in Figure 4. They are grouped mostly in the nightside magnetosphere. The bursts had not been observed when Interball 2 was orbiting in the dayside magnetosphere. This suggests that they are not generated on the dayside and the emission cones of the nightside AKR bursts are rather narrow.

Examination of the low-frequency limits of the AKR bursts shows that they were always higher than the electron gyrofrequency at the Interball 2 location, and therefore no source crossing was met. However, for a number of bursts, rapid increases of the keV electron fluxes, together with rather weak field-aligned currents (a few μA m^{-2} at the ionospheric level), and a ULF wave activity were observed with the onboard instruments: ION [*Sauvaud et al.*, 1998], IMAP-3 [*Arshinkov et al.*, 1995], and IESP [*Perraut et al.*, 1998] (Figure 4,

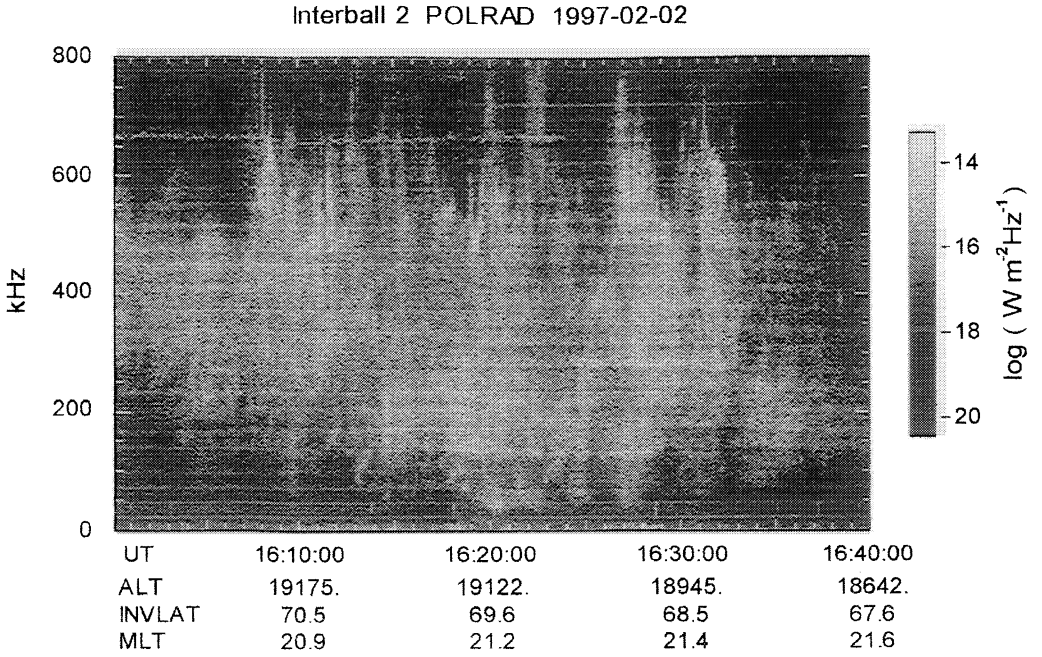

Figure 3. Example showing microbursts of AKR.

solid circles), indicating that at these times the spacecraft entered regions magnetically conjugated to auroral bulges, although it passed beside the AKR sources. In Figure 4 the spacecraft positions for these cases are marked by solid circles. They are concentrated in the pre-midnight sector of the magnetosphere, thus suggesting that the sources are likely to be located in the western part of the auroral bulges. The onsets of these electron and ULF wave events, which may follow the AKR bursts by a few minutes (< 10 min), indicate that the spacecraft enters with some delay the disturbed regions conjugated to the auroral bulges.

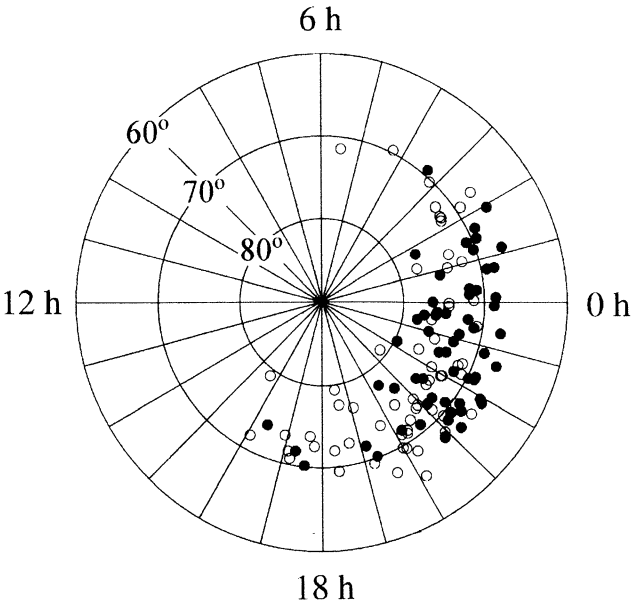

Figure 4. Magnetic local time (MLT) positions of Interball 2 at times of AKR bursts; solid circles show bursts associated with wave-particle events; open circles show no association.

3. Association With Auroral Structures

The UV imager operates on the Polar spacecraft in the far ultraviolet and has an 8° circular field of view with 0.6 mrad per pixel resolution, with a nominal frame rate of 1 frame every 37 s [*Torr et al.*, 1995]. Sixty-five AKR bursts were recorded during periods when the UV imager was operating. All but two were associated with the expansion and simultaneous brightening of auroral bulges.

We shall show evidence that the AKR bursts are triggered during the development of the auroral substorms, when the auroral bulge structures are in a rapid expansion at the ionospheric altitude. The dynamics of their evolution is illustrated in Plate 3 and shows three subsequent UV images of the bulge taken in the time interval just before and just after the time of the WBB-AKR shown in Plate 2. The footprint of the Interball 2 field line is indicated by a cross. The burst emission was associated with the explosive poleward expansion and brightening of the bulge, which took place between 1510:36 and 1512:08 UT. At the time of the first image the spacecraft footprint was at the edge of the rising bulge, whereas 1.5 min. later it was already surrounded by the bulge, just at the edge of its bright core. The latter was coincident with the onsets of the ULF turbulence detected by the IESP instrument (1512:00 UT) [*Perraut et al.*, 1998] and of the energetic electron flux, up to 10 keV, recorded by the ION instrument (1512:30 UT) on board of Interball 2.

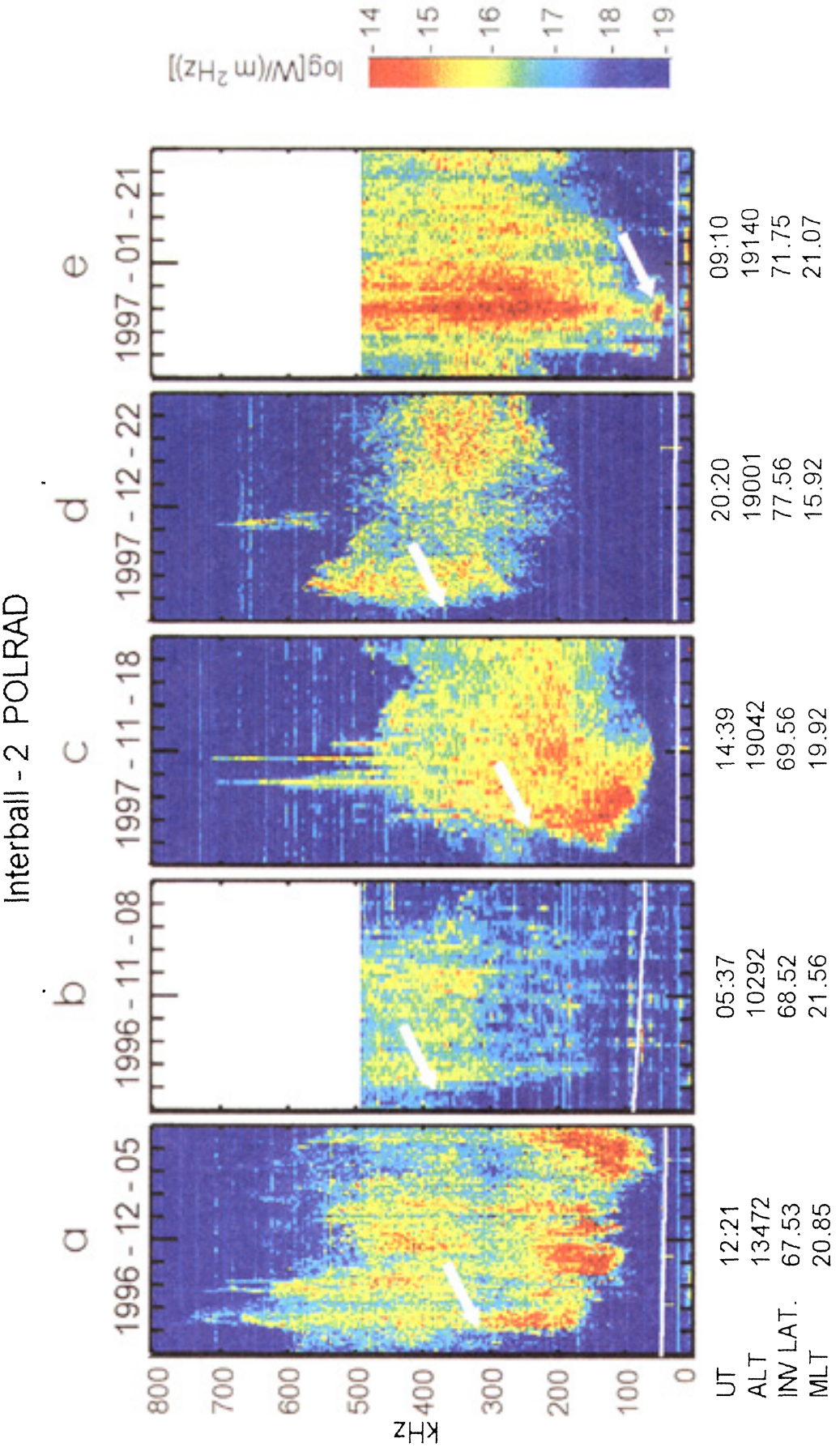

Plate 1. Examples of different types of bursts of auroral kilometric radiation (AKR) observed by POLRAD (POLarization of RADioemission) aboard Interball 2. Time is marked every minute. Decimal logarithms of power density are marked on the color scale. Local electron gyrofrequency is shown by the white line. (a) Burst with unmeasurable high drift rate (December 5, 1996, 1217 UT). (b) Burst with a negative drift rate (November 8, 1996, 0533 UT). (c) Burst with a positive drift rate (November 18, 1997, 1435 UT). (d) Burst with a "bow" front edge (December 22, 1997, 2016 UT). (e) "exclamation sign" burst with a detached spot (January 21, 1997, 0907 UT).

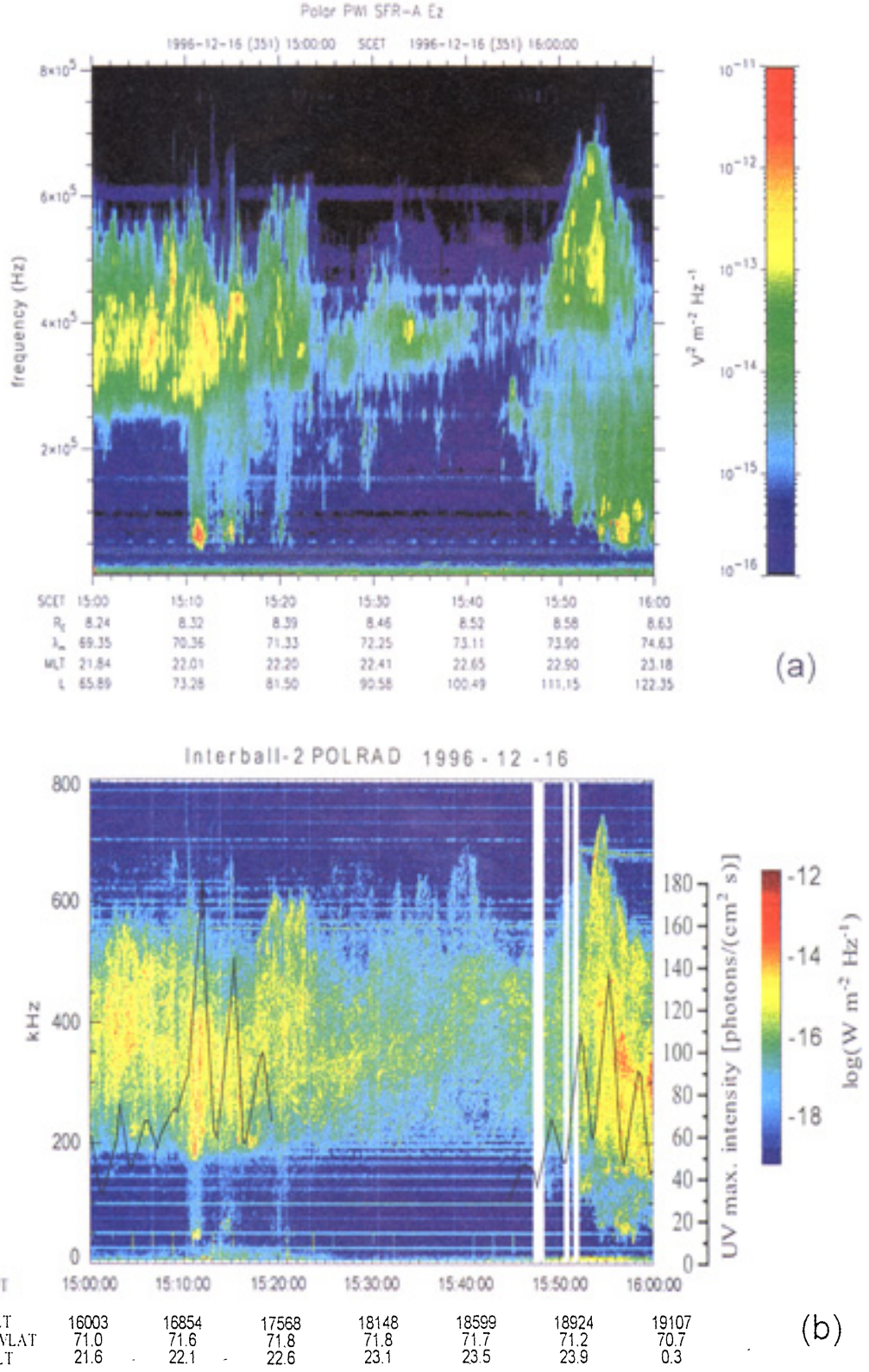

Plate 2. Bursts of AKR observed simultaneously by (a) PWI from Polar and (b) POLRAD from Interball 2. Superimposed in the bottom panel is the plot of the UV photon flux variations of the brightest pixel within the bulge area, as measured from the UV imager on Polar. Spectrogram in upper panel is provided courtesy of D. Gurnett.

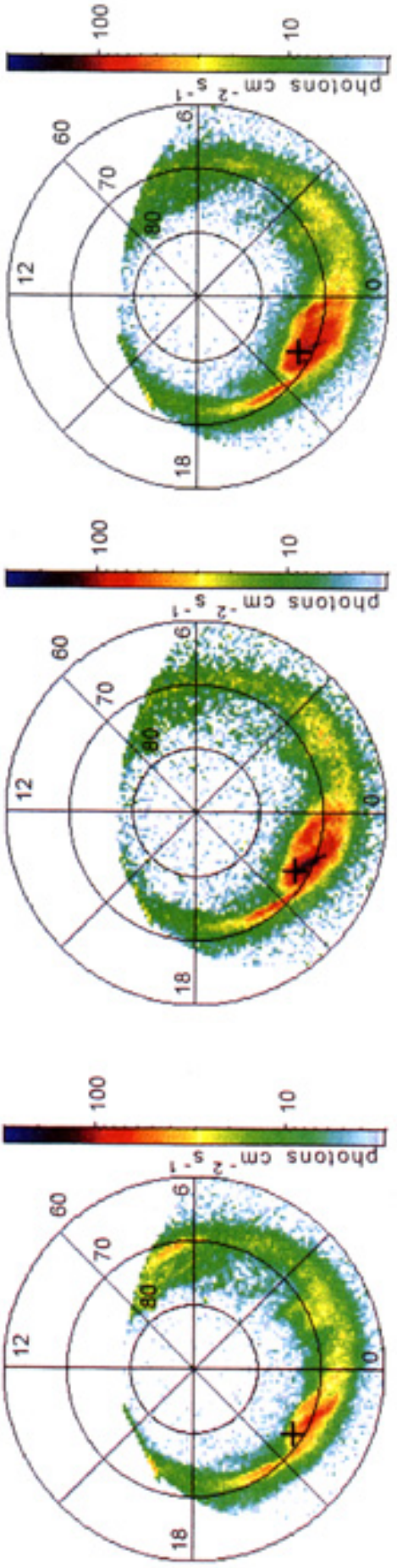

Plate 3. Sequence of UV images (LBHL - Lyman-Birge-Hopfield Long wavelength filter) from Polar showing development of the auroral bulge associated with the AKR burst on December 16, 1996, 1511 UT. (a) Time 1510:36 UT, just prior to the burst onset, (b) time 1512:08 UT, just at the end of the burst, (c) time 1512:27 UT, 35 s after the end of the burst. The cross indicates the location of the footprint of the Interball 2 field line.

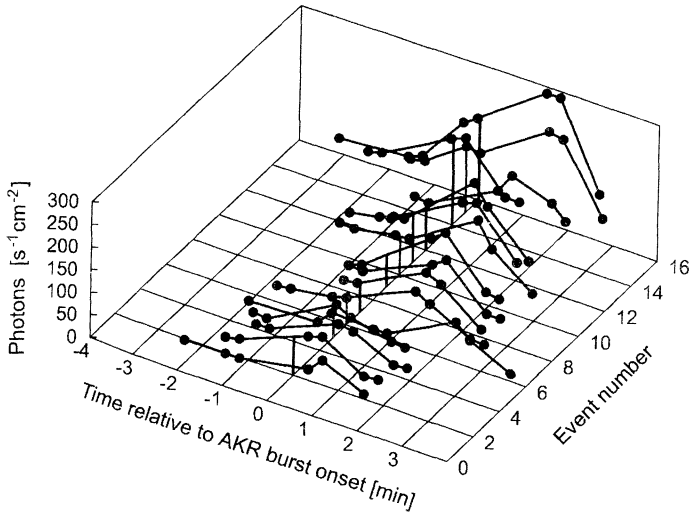

Figure 5. Variations of intensity of the brightest point of the bulge taken for 16 sequences of UV images from Polar, as a function of time difference between the UV exposure and burst onset. Vertical segments are drawn in cases when enhanced UV flux measurement preceded the burst onset.

It is evident from the bottom panel of Plate 2 and Figure 5 that the triggering of the AKR takes place at a brightening phase of the bulge development. The bottom panel of Plate 2, which shows photon flux variations of the brightest pixel within the bulge area overlayed on the dynamic spectrum of AKR, is a good example of a time coincidence of WBB-AKR with sudden brightening of the auroral bulge. Figure 5 shows the light variations for the 16 brightest observed bulges. In 10 cases (pointed with the vertical segments) the first noticeably enhanced UV flux measurement preceded the burst onset by 1 - 2 min. In another six cases it followed the burst onset by less than 1 min, and could easily be missed since the time intervals between two subsequent UV images were too long compared to the timescale of the bulge development. For the 16 cases analyzed the burst onset took place before (less than 1 min) or at the maximum of the UV flux. From the above observations we conclude that the AKR bursts are triggered during the rapid explosive expansion phase of the auroral substorms, after the onset of the auroral bulge and on the increasing part of its light curve.

4. Discussion

4.1. Sudden Onset and Decay

It is shown in section 2 that in the upper frequency range the intensity of the AKR bursts abruptly increases and further abruptly decreases by 1 - 3 orders of magnitude in a timescale of seconds. If, as it is usually assumed, the waves are generated by the cyclotron maser instability (CMI), the saturation level is reached in 1000 or 2000 gyroperiods of the electrons, that is, in a few milliseconds, as has been determined from particle simulations [*Winglee and Pritchett*, 1986].

The timescale of the free energy erosion by emission of the AKR has been determined from a particle simulation [*Winglee and Pritchett*, 1986] to be also of several thousands of gyroperiods. Then what we observe are waves generated by a saturated maser, and the increase or the decrease of the intensity is due to the variable saturation level. From the characteristic times given above one can expect that it is more or less directly related to the efficiency of the replenishment of the free energy source.

Broadly speaking, in terms of the distribution function, the condition $\partial f/\partial v_\perp > 0$ must be fulfilled in some area of the velocity space. There are three main classes of sources of free energy. One is the loss cone, which can be enhanced by the presence of a parallel electric field [*Bahnsen et al.*, 1989]. The efficiency of this source is probably too small to account for most of the observations. In a few words, this source needs a significant parallel wave number, with a corresponding parallel component of the phase velocity, which does not allow an efficient lasing in the source cavities. Moreover, the free energy loss should be restored in times comparable to several bounce periods for the keV electrons, which is too long compared to the rise time of the bursts.

A second source can be found in the so-called trapped particles [*Knight*, 1973], when a parallel potential drop is present. It has been shown that a trapping of electrons with perpendicular velocities is achieved, when a fluctuating electric field in the ULF range is present [*Eliasson et al.*, 1979]. Such ULF electric fields were met [*Perraut et al.*, 1998] when Interball 2 entered a region magnetically conjugated to the auroral bulges. With this mechanism the free energy losses would be restored in several characteristic times of the fluctuations,

that is, of the order of a second, which is acceptable for the bursts.

The last source can be found when downgoing electron beams are dispersed in the velocity space thanks to the conservation of the first adiabatic invariant. This situation has been simulated by *Winglee and Pritchett* [1986]. In their simulation, seemingly, the saturation results from the erosion of the perpendicular distribution function by the pitch angle diffusion of the electrons accompanying the wave emission. In such a situation it is expected that the increasing downgoing electron fluxes should supply the needed free energy and increase the saturation level.

The last two mechanisms, that is, (1) electron trapping and (2) dispersion of the downgoing beams, are more likely. In the general context of the expansion phase of substorms the downgoing electron beams must play a prominent role, which favors the latter possibility for the burst sources. On the other hand, the recent work of *Génot et al.* [1999] shows that in a steep density gradient of the plasma density, by a factor of 3 over a distance of less than either the electron inertial length ω_p/c (ω_p -plasma frequency, c -speed of light) or the ion gyroradius, an incident Alfvén wave develops an inertial or kinetic behavior. The front of the wave packet stretches along the gradient, and a parallel electric field, as high as 1 mV m^{-1} (in the framework of a linear theory), can develop simultaneously over an altitude range of 16,000 km. This fits our observations of the AKR burst altitude range. (Génot et al.'s simulation gives even higher electric fields, but over smaller field-aligned distances due to a limited size of the simulation box.) Moreover, the peak value is obtained after $\sim$ 3000 ion gyroperiods, i. e., a few seconds. Then the second mechanism is most likely.

4.2. Expansion and Contraction of the Source Region

We have shown that the WBB-AKR is characterized by a frequency range broader than that of the background long-lasting AKR emissions. Assuming that the waves are generated at the electron gyrofrequency, and converting the frequency range into an altitude range for the source region, this broadening means that the bottom of the generation region penetrates deeper toward the Earth for the bursts than for the background AKR. A similar conclusion can hardly be drawn for the top of the generation region, since it is too close to the spacecraft and, in a first analysis, propagation effects cannot be easily disentangled.

The time evolution of the frequencies of the leading and trailing edges is evoked by the propagation of the source fronts. It has been converted to velocities of the source expansion and contraction; however, the nature of this motion is not known.

The source expansion derived from the frequency drift rates of the leading edge of the bursts has been divided into three parts. Each one can be driven by a different process. In the central part of the bursts (200 - 500 kHz), which is usually observed at the very beginning of the bursts, the estimated velocities are large and sometimes non-measurable, 3000 km s^{-1} or more, comparable to the Alfvén velocity.

In the upper frequency part, from 500 to 800 kHz, corresponding to altitudes from 1700 to 3000 km, the velocities of the leading and trailing edges of the source region are much lower, of the order of 2 - 30 km s^{-1}, and often stay fairly constant along a 500 - 1000 km change in altitude. The order of magnitude is that of the ion acoustic velocity, but this might be a mere coincidence. If the observed velocity, as low as 2.3 km s^{-1}, were an ion acoustic velocity, then the electron temperature should be 0.05 eV at an altitude 2700 km, which is obviously too small.

The negative frequency drift rate in the lower frequency range, below 200 kHz, may correspond to an upward expansion of the source region. However, since the altitude of the source region is comparable to that of the spacecraft, the lower cutoff frequency of the bursts can be subjected to a propagation effect.

4.3. Microstructure

The microstructure of the bursts shows that the full frequency range (30 - 800 kHz) of each individual microburst can excite within a few seconds and fade out as quickly as they are excited. This has two consequences: the first one is that the AKR bursts are the signature of "macroprocesses" embedding the microbursts, which start suddenly, grow up within 1 or 2 min, and relax in a few tens of minutes. Their overall extension reaches an altitude range of 2000 - 20,000 km. Today, we have no means to assess their horizontal cross section. The nature of these macroprocesses will be made clearer in the section 4.4.

The second consequence is that the overall source region is filamented in a bunch of subsources, which are switched on and off with a time separation of the order of 10 s. The above mentioned work by *Génot et al.* [1999] shows that the transverse size of the current filaments may reach extremely small scales, similarly as the edges of the AKR sources observed by Viking [*de Feraudy et al.*, 1987b].

This filamentation may possibly be related to the filamentation of a broader field-aligned current (FAC). Until now the association of the AKR to FACs has only been made at a macroscale by *Green et al.* [1982], who have shown from the observations of Hawkeye and Triad spacecraft a broad correlation between the global AKR activity and the intensity of the large-scale currents. However, these authors noted that most probably the appropriate scale is a microscopic one. The Interball 2 observations suggest that it may be the scale of the AKR individual sources, that is a few tens of kilometers in accord with the Viking observations [*de Feraudy e*

al., 1987b], which also corresponds to FAST observations [*Ergun et al.*, 1998].

4.4. Association With Substorm Development and Auroral Bulge Expansion

The availability of high-resolution auroral images in the UV range, from the Polar Ultraviolet Imager (UVI) experiment, have enabled us to place our observations in the frame of the substorm development. More specifically, we have shown in Plate 3 and Figure 5 the close association of the AKR bursts with the fast expansion of the auroral bulge. The association is substantiated by the fact that the duration of the full vertical expansion of the AKR burst sources, related to the burst frequency drift, is of the order of 1 min. This is comparable to the time of the poleward expansion of the auroras which are observed from Meridian Scan Photometers (a clear example is shown by *Deehr* [1994]).

Today, it is widely admitted that the auroral bulge expansion is associated with the disruption of tail currents and with the onset of a current wedge (for instance, see the review from *Lui* [1996]. The closure of the current wedge system involves upflowing currents at its western end. The fast expanding auroral bulge is, seemingly, the ionospheric trace of its development (its western part is sometimes identified as a "westward traveling surge"). The most intense part of the bulge UVI images is likely to be located at the footprint of these field-aligned currents, and it is reasonable to assume that it is also the projection of the AKR burst source region onto the ionosphere. In this hypothesis the microstructure of the AKR bursts is the signature of a current filamentation.

5. Conclusions

1. The wideband bursts of AKR, observed from Interball 2, establish the specific kind of AKR emission. They are characteristic for the rapid intensity onset in a timescale of less that 1 min, and for the fast frequency drift rate of their leading edges, positive or negative, spanning from 3 to $>$ 100 kHz, in a timescale of the order of 1 s. Their frequency range is wide, from 30 to 900 kHz. They are short-lived, with the decay times of tens of minutes. In the upper frequency range, above $\sim$ 500 kHz, their lifetimes are shorter, and the rise time and the decay time are of the order of 10 s.

2. The wideband AKR bursts are clearly triggered during the rapid poleward expansion phase of substorms, manifested by development of the auroral bulges.

3. Loci of the burst observations, related to the limited extent of the AKR cone emission, indicate that the sources of the bursts are most frequently encountered in regions conjugated to the western part of the auroral bulges, which are also the places where the auroral UV emissions are the most intense.

4. If the bulge development is associated with the onset of a current wedge, then upflowing current regions, corresponding to downflowing electrons, must be collocated with the bursts' sources.

5. The AKR bursts exhibit a microstructure of very short lived sources, which have a long extension along the field lines, of the order of 10,000 km. As it has been observed by Viking and FAST, their transversal dimension should be of the order of tens of kilometers. They are rapidly switched on and off during the bursts events.

6. Provided that the source structures can be associated with the field-aligned upflowing wedge current region, the microstructure of the AKR bursts reflects a filamentary and time-fluctuating structure of the current system.

Acknowledgments. The authors are grateful to D. A. Gurnett for permission to use Polar PWI spectra and to S. Perraut, J. A. Sauvaud, V. A. Styazhkin, and A. Bochev for permission to use the measurements of the wave turbulence (IESP), energetic spectra of electrons (ION), and magnetic field (IMAP-3), received from Interball 2. The authors are very thankful to the referees for their criticism and helpful suggestions. They would also like to thank H. Launay and M. Małycha for their help in data analysis. The Polish space experiment POLRAD, carried out by the Space Research Centre (Poland) has been developed together with the Copernicus Astronomical Centre and the Institute of Aviation. The Space Research Institute (Moscow), Russian Space Agency, Lavochkin Space Association, and Babakin Centre made Interball a reality. Part of the POLRAD data was received at the telemetry station of Panska Ves (Czech Republic). Thanks are due to Joelle Durand and her team (CNES Toulouse) for processing the POLRAD data. This work was financially supported by the Committee of the Scientific Research in Poland, grant 2 P03C 003 16 and the program of Polish-French integrated actions Polonium 2000 98213.

Michel Blanc thanks Michael Kaiser and another referee for their assistance in evaluating this paper.

References

Acuña, M. H., K. W. Ogilvie, D. N. Baker, S. A. Curtis, D. H. Fairfield, and W. H. Mish, The Global Geospace Science Program and its investigations, *Space Sci. Rev., 71*, 5, 1995.

Anderson, R. R., et al., Observations of low frequency terrestrial type III burts by Geotail and Wind and their association with isolated geomagnetic disturbances detected by ground and space-borne instruments, in *Planetary Radio Emissions IV*, edited by H. O. Rucker, S. J. Bauer, and A. Lecacheaux, p. 241, Verlag der Österreichischen Akad. des Wiss., Graz, Austria, 1996.

Arshinkov, I. S., Z. N. Zhuzgov, A. Bochev, E. Zahkareva, V. Velev, V. A. Styazhkin, P. T. Baynov, and N. Abadgiev, Magnetic field experiment in the INTERBALL project (experiment IMAP), in *Interball: Mission and payload*, CNES, Paris, p. 222, 1995.

Bahnsen, A., B. Pedersen, M. Jespersen, E. Ungstrup, L. Eliasson, J. Murphree, R. Elphinstone, L. Blomberg, G. Holmgren, and L. J. Zanetti, Viking observations at the source region of auroral kilometric radiation, *J. Geophys. Res., 94*, 6643, 1989.

Benediktov, E. A., G. Getmantsev, Y. A. Sazonov, and A. F. Tarasov, Preliminary results of measurements of the intensity of distributed extra-terrestrial radio frequency

emission at 725 and 1525 kHz (in Russian), *Kosm. Issled., 3*, 614, 1965.

Benson, R. F., and S.-I. Akasofu, Auroral kilometric radiation / aurora correlation, *Radio Sci., 19*, 527, 1984.

Benson, R. F., and W. Calvert, ISIS-1 observations of the source of AKR, *Geophys. Res. Lett., 6*, 479, 1979.

Deehr, C. S., Ground-based optical observations of hydrogen emissions in the auroral substorm, in *2nd International Conference on Substorms*, edited by S.-I. Akasofu, p. 229, Fairbanks, Alaska, 1994.

de Feraudy, H., A. Bahnsen, and M. Jespersen, Observations of nightside and dayside auroral kilometric radiation, in *Planetary Radio Emissions II*, edited by H. O. Rucker, S. J. Bauer, and B. M. Pedersen, p. 41, Verlag der Österreichischen Akad. des Wiss., Graz, Austria, 1987a.

de Feraudy, H., B. Pedersen, A. Bahnsen, and M. Jespersen, Viking observations of auroral kilometric radiation from the plasmasphere to night auroral oval source regions, *Geophys. Res. Lett., 14*, 511, 1987b.

Desch, M. D., Terrestrial LF bursts source and solar wind connection, in *Planetary Radio Emissions IV*, edited by H. O. Rucker, S. J. Bauer, and A. Lecacheaux, p. 251, Verlag der Österreichischen Akad. des Wiss., Graz, Austria, 1996.

Eliasson, L., G. Holmgren, and K. Rönnmark, Pitch angle and energy distribution of auroral electrons measured by the ESRO-4 satellite, *Planet. Space Sci., 87*, 2345, 1979.

Ergun, R. E. et al., FAST satellite observations in the AKR source region, *Geophys. Res. Lett., 25*, 2061, 1998.

Galeev, A. A., Y. I. Galperin, and L. M. Zelenyi, The Interball project to study solar - terrestrial physics, in *Interball: Mission and payload*, CNES, Paris, p. 11, 1995.

Génot, V., P. Louarn, and D. Le Queau, A study of the propagation of Alfvén waves in the auroral density cavities, *J. Geophys. Res., 104*, 22,649, 1999.

Green, J. L., N. A. Saflekos, D. A. Gurnett, and T. A. Potemra, A correlation between auroral kilometric radiation and field-aligned currents, *J. Geophys. Res., 87*, 10,467, 1982.

Gurnett, D. A., The Earth as a radio source: Terrestrial kilometric radiation, *J. Geophys. Res., 79*, 4227, 1974.

Gurnett, D. A., et al., The Polar Plasma Wave Instrument, *Space Sci. Rev., 71*, 597, 1995.

Hanasz, J., et al., Observations of auroral kilometric radiation on board Interball-2: Polrad experiment, *Cosmic Res., 36*, Engl. Transl., 575, 1998a.

Hanasz, J., R. Schreiber, H. de Feraudy, M. M. Mogilevsky, and T. V. Romantsova, Observations of the upper frequency cutoffs of the auroral kilometric radiation, *Ann. Geophys., 16*, 1097, 1998b.

Huff, R. L., W. Calvert, J. D. Craven, L. A. Frank, and D. A. Gurnett, Mapping of Auroral Kilometric Radiation Sources to the Aurora, *J. Geophys. Res., 93*, 11445, 1988.

Imhof, W. L., D. L. Chenette, D. W. Datlowe, and J. Mobilia, The correlation of AKR waves with precipitating electrons as determined by plasma wave and x-ray image data from the Polar spacecraft, *Geophys. Res. Lett., 25*, 289, 1998.

Kaiser, M. L., and J. K. Alexander, Relationship between auroral substorms and the occurrence of terrestrial kilometric radiation, *J. Geophys. Res., 82*, 5283, 1977.

Kaiser, M. L., M. D. Desch, W. M. Farrell, J.-L. Steinberg, and M. J. Reiner, LF band terrestrial radio bursts observed by Wind/WAVES, *Geophys. Res. Lett., 23*, 1283, 1996.

Knight, S., Parallel electric fields, *Planet. Space Sci., 21*, 741, 1973.

Kurth, W. S., M. M. Baumback, and D. A. Gurnett, Direction finding measurements of auroral kilometric radiation, *J. Geophys. Res., 80*, 2764, 1975.

Lui, A. T. Y., Current disruption in the Earth's magnetosphere: observations and models, *J. Geophys. Res., 101*, 13,067, 1996.

Morioka, A., H. Oya, and S. Miyatake, Terrestrial kilometric radiation observed by satellite Jikiken (Exos-B), *J. Geomagn. Geoelectr., 33*, 37, 1981.

Perraut, S., A. Roux, F. Darrouzet, C. de Villedary, M. Mogilevsky, and F. Lefeuvre, ULF wave measurements on board the Interball Auroral Probe, *Ann. Geophys., 16*, 1105, 1998.

Sauvaud, J. A., H. Barthe, C. Aoustin, J. J. Thocaven, J. Rouzaud, E. Penou, D. Popescu, R. A. Kovrazhkin, and K. G. Afanasiev, The ion experiment on board the Interball-Aurora satellite; initial results on velocity-dispersed structures in the cleft and inside the auroral oval, *Ann. Geophys., 16*, 1056, 1998.

Steinberg, J.-L., C. Lacombe, and S. Hoang, A new component of Terrestrial Radio Emission observed from ISEE-3 and ISEE-2 in the solar wind, *Geophys. Res. Lett., 15*, 176, 1988.

Torr, et al., A far ultraviolet imager for the International Solar-Terrestrial Physics Mission, *Space Sci. Rev., 71*, 329, 1995.

Voots, G. R., D. A. Gurnett, and S.-I. Akasofu, Auroral kilometric radiation as an indicator of auroral magnetic disturbances, *J. Geophys. Res., 82*, 2259, 1977.

Winglee, R. M., and P. L. Pritchett, The generation of low-frequency electrostatic waves in association with auroral kilometric radiation, *J. Geophys. Res., 91*, 13,531, 1986.

Wu, C. S., and L. C. Lee, A theory of the terrestrial kilometric radiation, *Astrophys. J., 230*, 621, 1979.

Zelenyi, L. M., and J.-A. Sauvaud, Interball-2: First scientific results, *Ann. Geophys., 16*, 1043, 1998.

M. Brittnacher and G. Parks, University of Washington, Geophysics Program, Box 351650, Seattle, WA 98195-1650.

H. de Feraudy, Centre d'Etude des Environnements Terrestre et Planetaires, CNRS, 10-12, Av. de l'Europe, 78140 Velizy, France.

J. Hanasz, Space Research Center PAS, ul. Rabiańska 8, PL 87-100 Toruń, Poland. (jhanasz@ncac.torun.pl)

M.M. Mogilevsky and T.V. Romantsova, Space Research Institute RAS, ul. Profsoyuznaya 84/36, 117810 Moscow, Russia.

R. Schreiber, Copernicus Astronomical Center PAS, ul. Rabiańska 8, PL 87-100 Toruń, Poland.

(Received December 12, 1999; revised June 9, 2000; accepted June 19, 2000.)